Electron-impact-excitation cross sections for electronic levels in neon for incident energies between 25 and 100 eV

D. F. Register, S. Trajmar, and G. Steffensen
Jet Propulsion Laboratory, California Institute of Technology, Pasadena, California 91109

David C. Cartwright
Los Alamos National Laboratory, University of California, Los Alamos, New Mexico 87545
(Received 1 February 1983)

Absolute differential cross sections (DCS's) for electron-impact excitation of the lowest forty electronic levels in atomic neon have been determined for incident electron energies of 30 and 50 eV, for the four lowest levels at 25 eV, and two levels at 100 eV. The cross sections for these forty electronic levels are grouped into fifteen features, six of which represent excitation to resolved single electronic levels and the remaining nine which contain the unresolved contributions from two or more electronic levels. These DCS's were extrapolated to 0° and 180° and integrated to yield absolute integral cross sections as a function of incident electron energy. The results are compared to other experimental and theoretical results.

I. INTRODUCTION

During the past eight years, the increased interest in the characteristics of electron scattering by rare-gas atoms has coincided with the development of the rare-gas halide class of lasers. This class of lasers (e.g., KrF and XeCl), of considerable practical interest because their wavelengths are in the near ultraviolet spectral region and their efficiency is relatively high, has electron-impact excitation of rare-gas halogen-donor mixtures[1] as the primary pumping mechanism. Optimization of the output power and efficiency of these lasers has, however, been handicapped by the absence of the electron-impact cross-section information required for detailed modeling. The bulk of the available electron collision cross-section data for rare-gas targets, reviewed by Bransden and McDowell,[2] are for helium and relatively little has been reported for the heavier atoms. An extensive investigation of the electron scattering characteristics of the rare-gas atoms (Ne, Ar, Kr, and Xe) is in progress, and detailed results for scattering by argon[3,4] and krypton[4,5] have recently been reported. Elastic scattering of electrons by neon has been discussed in the preceding paper[6] and inelastic scattering of electrons by neon atoms, for incident electron energies in the range 25—100 eV, is the subject of this paper.

Some of the earliest work on neon is contained in the classic series of papers by Nicoll and Mohr who appear to be the first to have reported differential cross sections (DCS's) for electronic excitation of neon[7] (although their results were for a single transition only). Forty years then elapsed before any new work on the DCS's for neon were reported. These new results included relative DCS's for the lowest four excited levels[8] and relative DCS's for a number of partially resolved features[9] in electron energy-loss spectra corresponding to excitation of groups of electronic levels. The DCS's reported here are absolute and, as a result of improved experimental techniques, contain more information about excitation of individual electronic levels, over a larger incident electron range, than previous work.

The information currently available on electron scattering by neon atoms is dominated by results on integral and total scattering cross sections. A summary of total scattering, excitation, ionization, and elastic cross sections based on a semiempirical method and all available data from 20—3000 eV electron-impact energies has been provided by de Heer *et al.*[10] and new measurements of the total cross sections have been reported by Wagenaar and de Heer[11] and by Kauppila *et al.*[12]

In this paper, absolute differential and integral cross sections for excitation of 16 features in the electron energy-loss spectrum of neon (composed of the lowest 40 electronic levels of neon) are reported for incident electron energies of 25, 30, 50, and 100 eV and for scattering angles from 10° to 140°. A summary of the theoretical work to which these results are compared is contained in the following article.[13]

II. EXPERIMENTAL APPARATUS AND PROCEDURES

A. Instrumentation

The electron-impact spectrometer used in these measurements has been described in detail elsewhere by Jensen[14] and by Trajmar and Register.[15] It consists of a vacuum chamber with internal magnetic shielding (less than 1-mG residual field at the scattering center) containing residual double hemispherical electron source and detector systems. All lenses in the electron optics are of cylindrical design (of gold-plated oxygen-free copper) with 0.005-in.-thick molybdenum apertures. The electron gun is differentially pumped to eliminate gas dependent effects. Base pressure of the vacuum vessel is $\approx 2\times 10^{-8}$ Torr and is usually reached within 10 hours of pumping. Typical operating pressures are $\approx 5\times 10^{-6}$ Torr with gas flowing

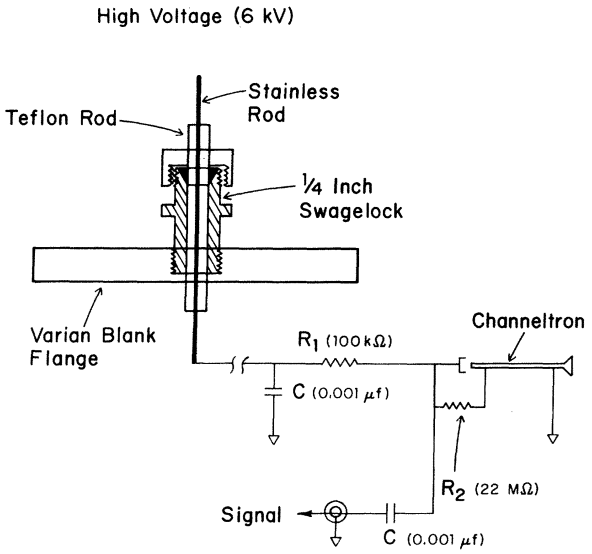

FIG. 1. Schematic diagram of the low-noise feed-through and signal-coupling circuitry used in the acquisition of the neon electron energy-loss data reported here.

in the system.

The gas flow system consists of a high-pressure gas source of spectroscopic purity (99.99% pure), a variable leak valve (Granville-Phillips), and a capacitance monometer (mks type 221A). The target beam is formed by a small capillary array (0.030-in. total array diameter) press fit into a 0.125-in.-diam-thick wall, nonmagnetic, stainless-steel tube. The array (100:1 aspect ratio, 200-in. overall length) is placed 0.125 in. below the scattering center and is operated at a back pressure of 2—4 Torr. At these pressures the flow is neither completely molecular nor viscous and care must be taken to properly account for geometric beam spreading.[16]

Although the multichannel scaler (MCS) (ND-600) and data-handling system (Tektronix 4052) are standard, the electronic amplifier and high-voltage systems have some special features as shown schematically in Fig. 1. The Channeltron high-voltage power supply is a Bendix PS400 unit bolted directly to a high-voltage vacuum feedthrough and enclosed in a grounded metal box. The power supply itself is of solid-state construction and has been found to

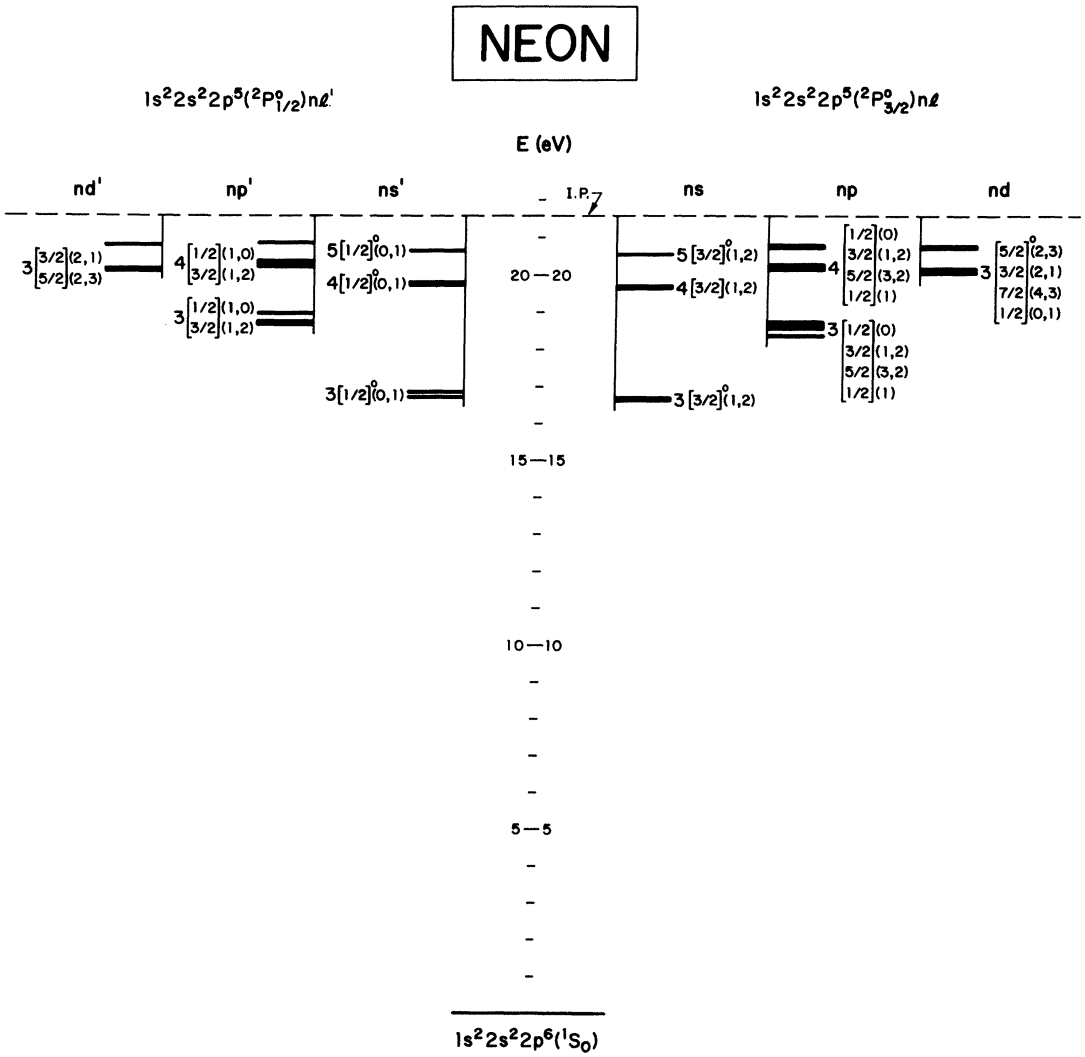

FIG. 2. Electron energy-level diagram for atomic neon produced from the spectroscopic data compiled by C. E. Moore, *Atomic Energy Levels,* Natl. Bur. Stand. (U.S.) Circ. No. 467 (U.S. GPO, Washington, D.C. 1948).

be exceptionally reliable and noise free. The proximity of the supply to the feedthrough virtually eliminates noise problems associated with high-voltage cables. Commercially available feedthroughs were found to be unacceptably noisy due to surface contamination of the ceramic insulators. An inexpensive and noise-free feedthrough was constructed by mounting a $\frac{1}{4}$-in. Swagelok bulkhead fitting on a standard $2\frac{1}{2}$-in. Varian blank flange. This fitting was reamed to $\frac{1}{4}$-in. i.d. and fitted with $\frac{1}{4}$-in.-o.d. Teflon rod which had been axially bored to accept a $\frac{1}{8}$-in.-o.d. stainless-steel rod fitted with 0.063-in. gold-plated Winchester connectors at either end. The assembly was sealed using standard Teflon Swagelok ferrules. Figure 1 illustrates the details of this low-noise feedthrough and the associated signal-coupling circuitry.

The high-voltage divider network is a standard configuration but has been mounted inside the vacuum chamber to further reduce noise problems. The 100-KΩ resistor and first 0.001-μfd capacitor act as an RC filter to prevent discharge noise from the power supply or feedthrough from reaching the signal output line. The second capacitor blocks the high voltage from the signal line and presents a low impedance (~ 1 Ω) to fast channeltron pulses. The signal line is a double-insulated 50-Ω coaxial cable which reduces the distributed capacitance in the system and allows one to utilize the inherent risetime advantages of the Channeltron electron multiplier (CEM) (Bendix Electro-Optics Technical Application Note No. 9803). The calculated mean pulse height and risetime associated with this system (~ 50 mV and 2 nS, respectively) was, in fact, realized.

The output pulse was fed to a low-noise, dual-stage, zero-walk, preamplifier (Avantek 6PD-402) located at the vacuum feedthrough. The input and output of this device are 50-Ω compatible. The preamplifier output was fed to a constant fraction discriminator (ORTEC), then to an emitter-coupled logic (ECL) amplifier, and then to a transitor-transitor logic (TTL) level converter for pulse shaping into the MCS unit. Although this system at first glance may seem cumbersome there are several distinct advantages: (1) The care paid to the high-voltage system greatly reduces the major source of noise present in most CEM systems, (2) the 50-Ω cabling not only preserves the CEM risetime, but also allows for significantly higher pulse amplitudes, and (3) the larger amplitude pulses allow more appropriate discriminator settings (~ 2 mV) than can be achieved with photon counting systems that have been adapted to electron detection. The resulting payoff for this effort is an efficient electron detection system with an observed system background count rate of 0.01 Hz. Since some of the cross sections in this and related work are as low as 10^{-23} cm^2/sr, the very low experimental background count allows for long data accumulation times (~ 24 hours) with a significant signal-to-noise advantage.

B. Experimental procedure

In addition to the instrumentation already described, several novel features were exploited in both the acquisition and analysis of the present data. Electron energy-loss spectra of neon (and similarly for all the rare gases) exhibit a large energy gap between elastic scattering and the first inelastic manifold which is illustrated diagrammatically in Fig. 2. There is a similar, but smaller, gap between these first four inelastic features and the next group of features associated with the higher electronic states. (The various spectroscopic identifications, the energy location, and electronic configuration of the lowest 40 excited

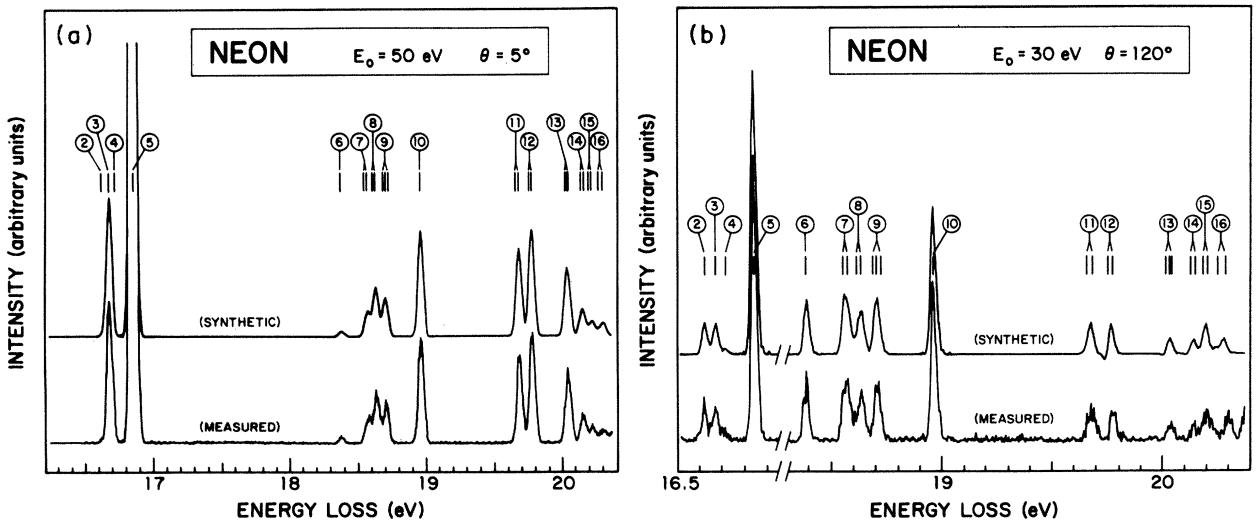

FIG. 3. (a) Electron energy-loss spectrum in neon for an incident electron energy of $E_0=50$ eV and a scattering angle of $\theta=5°$. The lower trace is the measured spectrum and the upper trace is the synthetic spectrum from which the contribution by excitation of various electronic levels, to each energy-loss feature, is determined. The circled numbers along the top of the figure correspond to the spectral feature numbers given in column 6 of Table I and serve only to identify the inelastic features. (b) Same as for (a) except for $E_0=30$ eV and $\theta=120$ degrees. Note that the energy-loss scale (b) differs from that in (a).

TABLE I. Spectroscopic identifications and locations[a] of the excited states of neon.

Paschen notation	Configuration	Designation[b]	J[b]	Energy (eV)	c	d
	$2p^6$	$2p^6\ {}^1S$	0	0	1	^1S_o
$1s_5$	$2p^5(^2P^o_{1\frac{1}{2}})3s$	$3s[1\frac{1}{2}]^o$	2	16.619	2	$^3P_2$
$1s_4$			1	16.671	3	$^3P_1$
$1s_3$	$2p^5(^2P^o_{\frac{1}{2}})3s$	$3s'[\frac{1}{2}]^o$	0	16.716	4	$^3P_0$
$1s_2$			1	16.848	5	$^1P^o_1$
$2p_{10}$	$2p^5(^2P^o_{1\frac{1}{2}})3p$	$3p[\frac{1}{2}]$	1	18.382	6	$^3S_1$
$2p_9$	"	$3p[2\frac{1}{2}]$	3	18.556	7	$^3D_3$
$2p_8$			2	18.576		$^3D_2$
$2p_7$	"	$3p[1\frac{1}{2}]$	1	18.613	8	$^3D_1$
$2p_6$			2	18.637		$^1D_2$
$2p_3$	"	$3p[\frac{1}{2}]$	0	18.712		$^3P_0$
$2p_5$	$2p^5(^2P^o_{\frac{1}{2}})3p$	$3p'[1\frac{1}{2}]$	1	18.694	9	$^1P_1$
$2p_4$			2	18.704		$^3P_2$
$2p_2$	"	$3p'[\frac{1}{2}]$	1	18.727		$^3P_1$
$2p_1$			0	18.966	10	$^1S_0$
$2s_5$	$2p^5(^2P^o_{1\frac{1}{2}})4s$	$4s[1\frac{1}{2}]^o$	2	19.664	11	---
$2s_4$			1	19.689		
$2s_3$	$2p(^2P^o_{\frac{1}{2}})4s$	$4s'[\frac{1}{2}]^o$	0	19.761	12	
$2s_2$			1	19.780		
$3d_6$	$2p^5(^2P^o_{1\frac{1}{2}})3d$	$3d[\frac{1}{2}]^o$	0	20.025		
$3d_5$			1	20.027		
$3d'_4$	"	$3d[3\frac{1}{2}]^o$	4	20.035		
$3d_4$			3	20.035	13	---
$3d_3$	"	$3d[1\frac{1}{2}]^o$	2	20.037		
$3d_2$			1	20.041		
$3d'_1{}'$	"	$3d[2\frac{1}{2}]^o$	2	20.049		
$3d'_1$			3	20.049		
$3s'_1{}'''$	$2p^5(^2P^o_{\frac{1}{2}})3d$	$3d'[2\frac{1}{2}]^o$	2	20.137		
$3s'_1{}''$			3	20.137	14	---
$3s'_1{}'$	"	$3d'[1\frac{1}{2}]^o$	2	20.138		
$3s'_1$			1	20.140		
$3p_{10}$	$2p^5(^2P^o_{1\frac{1}{2}})4p$	$4p[\frac{1}{2}]$	1	20.150		
$3p_9$	"	$4p[2\frac{1}{2}]$	3	20.189		
$3p_8$			2	20.197	15	---
$3p_7$	"	$4p[1\frac{1}{2}]$	1	20.211		
$3p_6$			2	20.215		
$3p_3$	"	$4p[\frac{1}{2}]$	0	20.260		
$3p_5$	$2p^5(^2P^o_{\frac{1}{2}})4p$	$4p'[1\frac{1}{2}]$	1	20.291	16	---
$3p_4$			2	20.298		
$3p_2$	"	$4p'[\frac{1}{2}]$	1	20.298		
$3p_1$			0	20.369		

[a]C. E. Moore, *Atomic Energy Levels,* Natl. Bur. Stand. (U.S.) Circ. No. 467 (U.S. GPO, Wahsington, D.C., 1952).
[b]The Paschen notation will be used in the text (see Ref. a).
[c]Resolved feature in the electron energy-loss spectra analyzed here.
[d]Term symbol appropriate for *LS* coupling. According to Ref. a above, the *LS* coupling description is really appropriate for only Paschen levels $2p_{10}$ through $2p_1$ but has been included for Paschen levels $1s_2$-$1s_5$ for purposes of qualitative identification.

levels in neon are summarized in Table I and correlated with the energy loss features in this study.) In order to improve the data collection efficiency, a simple electromechanical switch was used to pass over the uninteresting energy-loss regions.[15]

Using this technique, data on the relative spectral intensities were acquired by standard multichannel scaling methods. At least two measurements were made at each energy (25, 30, 50, and 100-eV impact energies) and each scattering angle ($-15°$ to $+140°$). Typical energy-loss spectra are shown as the lower traces in Fig. 3. The relative spectral intensities at each angle were converted to relative intensity distributions (as a function of scattering angle) by normalizing each feature to the intensity of the strong $1s_2(^1P_1)$ transition (feature 5 of Table I). This feature, in turn, was calibrated against the elastic DCS (Ref. 6) with particular care being taken to ensure that the detection efficiency of the electron optics was the same[16] for both the elastic and inelastic features.

The computer unfolding technique was similar to that used earlier by Cartwright *et al.*[17] and by Register *et al.*,[18] but with some improved features. In the present technique an isolated feature was chosen [usually the strong $1s_2(^1P_1)$ feature] as a reference peak. The shape of this feature was stored in a separate array and assumed to be characteristic of the overall system response for the energy-loss spectra under study. Once a reference feature was chosen, the energy scale of the spectra was calibrated and the position of all possible energy-loss features of interest was calculated (using Moore's tables; see Table I). The shape of the reference peak was applied to each of these positions and the height of all the spectral features calculated using a least-squares algorithm in a Gaussian reduction matrix solution. In this way as many as 27 spectral features, as well as the background, were evaluated simultaneously. Since a number of the levels were not resolved in the energy-loss data, they were grouped together to give the 15 features listed in Table I. The synthetic spectrum (upper traces) calculated by this procedure are compared with the appropriate measured spectrum (lower traces) in Fig. 3.

C. Error estimation

The errors associated with the present data arise from four possible sources: (1) normalization of the elastic DCS; (2) normalization of the reference inelastic feature [usually that corresponding to excitation of the $1s_2(^1P_1)$ level] against the elastic DCS; (3) normalization of the inelastic DCS against the reference inelastic feature; and (4) statistical and other uncertainties in the evaluation of the inelastic peak heights. In addition to these errors, further uncertainties arise in the extrapolation of the DCS's to 0° and 180° scattering angle for determining the integral excitation and momentum transfer cross sections. These errors are discussed below in order of increasing significance.

The uncertainties associated with the elastic DCS have been discussed previously and are taken as 10%. The normalization of the $1s_2(^1P_1)$ feature against the elastic feature introduces a comparable uncertainty (10%). For the inelastic features [other than the $1s_2(^1P_1)$], both the agreement among the different measurements for the same spectral feature and the statistical uncertainties in the observed count rates contribute comparable errors. These uncertainties are quite small for the strongest isolated features ($\sim 10\%$ for transitions such as feature 10 of Fig. 3) but are the dominant errors for the weakest and strongly blended features ($\sim 30\%$ for feature 4 of Fig. 3).

TABLE II. Electron-impact inelastic differential cross sections (10^{-19} cm^2/sr) for neon at $E_0=25$ eV.

	Feature number[a]			
	2	3	4	5
θ (deg)	$1s_5(^3P_2)$	$1s_4(^3P_1)$	$1s_3(^3P_0)$	$1s_2(^1P_1)$
10	1.72	3.17	—	29.6
15	1.50	2.76	0.287	24.3
20	1.66	2.44	0.291	19.0
30	1.72	1.80	0.398	11.2
40	1.84	1.51	0.416	6.0
50	1.45	0.948	0.280	2.73
60	1.33	0.899	0.294	1.70
70	1.14	0.734	0.235	1.07
80	0.815	0.438	0.162	0.66
90	0.704	0.393	0.138	0.75
100	0.452	0.319	0.112	0.95
110	0.322	0.238	0.114	1.08
120	0.227	0.198	0.071	1.17
130	0.314	0.254	0.060	1.41
140	0.308	0.256	0.080	1.43
% Error	15	15	22	13

[a]For explanation of feature numbers see Table I.

TABLE III. Electron-impact inelastic differential cross sections (10^{-19} cm^2/sr) for neon at $E_0=30$ eV.

	Feature[a]														
θ (deg)	2	3	4	5	6	7	8	9	10	11	12	13	14	15	16
5	1.66	11.79		136.0	0.109	1.723	3.80	3.01	11.05	3.72	4.37	3.46	1.52	1.14	1.59
10	1.99	9.43	0.466	104.0	0.331	2.08	3.56	3.2	10.21	3.60	3.80	3.16	1.30	1.19	1.35
15	2.05	6.89		72.5	0.276	1.86	3.26	3.33	8.12	3.24	3.31	2.57	1.18	1.15	1.26
20	2.06	5.23	0.663	49.1	0.162	1.80	3.39	3.57	6.37	2.49	2.39	2.28	0.914	1.17	1.13
30	1.84	2.17	0.399	14.0	0.031	1.21	1.62	1.91	2.23	1.00	0.757	0.841	0.368	0.604	0.611
40	2.01	1.64	0.319	6.9	0.077	1.21	1.22	1.35	1.62	0.863	0.666	0.538	0.420	0.570	0.653
50	1.79	1.19	0.395	3.51	0.137	1.07	0.116	1.00	1.02	0.647	0.325	0.277	0.143	0.447	0.335
60	1.38	1.04	0.319	1.99	0.254	0.809	0.645	0.792	1.19	0.596	0.318	0.282	0.156	0.420	0.318
70	1.30	0.94	0.304	1.64	0.253	0.977	0.601	0.773	1.63	0.581	0.322	0.374	0.177	0.437	0.310
80	0.84	0.59	0.174	1.29	0.154	0.728	0.574	0.767	1.91	0.481	0.220	0.273	0.127	0.400	0.287
90	0.42	0.34	0.097	1.17	0.101	0.515	0.48	0.515	1.53	0.222	0.174	0.174	0.109	0.291	0.226
100	0.65	0.26	0.093	1.52	0.149	0.382	0.461	0.589	1.42	0.228	0.193	0.131	0.076	0.232	0.238
110	0.17	0.19	0.036	1.64	0.221	0.452	0.419	0.522	1.06	0.247	0.210	0.118	0.101	0.301	0.210
120	0.21	0.24	0.051	1.87	0.408	0.529	0.429	0.474	0.98	0.257	0.207	0.116	0.096	0.241	0.181
130	0.17	0.22	0.040	1.64	0.471	0.415	0.334	0.398	0.804	0.235	0.213	0.104	0.161	0.178	0.162
135	0.19	0.22	0.043	1.64	0.690	0.321	0.366	0.323	0.927	0.259	0.173	0.129	0.194	0.172	0.194
140	0.17	0.23	0.044	1.64	0.630	0.435	0.321	0.321	1.12	0.240	0.189	0.151	0.220	0.233	0.189
% Error	19	17	35	15	27	19	19	17	18	20	21	23	25	23	20

[a]For definition of the feature numbers, see Table I.

TABLE IV. Electron-impact inelastic, differential cross sections (10^{-19} cm^2/sr) for neon at $E_0 = 50$ eV.

	Feature[a]														
θ (deg)	2	3	4	5	6	7	8	9	10	11	12	13	14	15	16
5	—	36.71	—	505.0	1.16	5.30	11.0	9.95	27.6	20.3	26.5	18.6	6.72	3.43	3.64
10	0.610	22.57	0.378	291.0	0.988	5.43	11.2	10.4	18.2	14.5	18.3	12.4	4.68	3.89	3.37
15	0.540	10.94	—	135.0	0.702	4.23	8.22	8.67	9.44	7.22	8.96	6.95	3.01	2.90	2.38
20	0.848	4.71	0.340	54.0	0.475	2.97	5.59	5.08	4.08	3.52	4.09	3.31	1.40	2.13	1.55
30	1.05	1.45	0.303	10.3	0.094	1.40	1.79	1.62	0.775	1.06	1.02	0.938	0.377	0.821	0.533
40	1.00	0.917	0.229	4.0	0.227	0.853	0.546	0.456	0.410	0.654	0.497	0.446	0.233	0.350	0.235
50	0.837	0.716	0.175	2.80	0.411	0.586	0.347	0.296	1.05	0.486	0.354	0.296	0.236	0.206	0.166
60	0.538	0.482	0.113	1.90	0.285	0.448	0.328	0.291	1.57	0.354	0.261	0.264	0.173	0.239	0.244
70	0.401	0.297	0.079	1.40	0.139	0.356	0.352	0.267	1.88	0.187	0.165	0.150	0.112	0.221	0.229
80	0.143	0.195	0.034	0.900	0.011	0.281	0.240	0.281	1.52	0.101	0.075	0.135	0.079	0.158	0.161
90	0.111	0.111	0.029	0.700	0.020	0.214	0.171	0.219	1.01	0.083	0.074	0.058	0.041	0.127	0.133
100	0.123	0.099	0.039	0.540	0.111	0.219	0.131	0.218	0.590	0.111	0.073	0.019	0.062	0.080	0.096
110	0.134	0.113	0.020	0.550	0.160	0.137	0.098	0.186	0.373	0.067	0.055	0.011	0.045	0.062	0.126
120	0.116	0.133	0.051	0.590	0.179	0.177	0.153	0.289	0.623	0.103	0.071	0.036	0.082	0.095	0.126
130	0.094	0.144	0.019	0.950	0.198	0.232	0.167	0.281	1.40	0.113	0.121	0.063	0.061	0.126	0.170
135	0.063	0.175	0.025	1.45	0.213	0.313	0.250	0.387	2.51	0.163	0.175	0.075	0.087	0.138	0.288
140	0.079	0.174	0.032	1.45	0.155	0.314	0.172	0.307	2.62	0.159	0.185	0.062	0.060	0.110	0.254
% Error	33	22	40	20	28	22	23	22	21	23	24	28	30	23	23

[a]For definition of the feature numbers, see Table I.

TABLE V. Electron-impact inelastic differential cross sections (10^{-19} cm^2/sr) for neon at $E_0 = 100$ eV.

	Feature number[a]	
θ (deg)	5 ($1s_2, {}^1P_1^o$)	10 ($2p_1, {}^1S_0$)
5	1033	45.4
10	272	16.8
15	70	6.8
20	17.8	1.8
30	3.3	0.48
40	1.6	0.84
50	0.98	1.07
60	0.62	0.98
70	0.34	0.65
80	0.22	0.37
90	0.14	0.13
100	0.08	0.047
110	0.14	0.068
120	0.23	0.38
130	0.49	0.91
140	0.81	1.67
% Error	20	20

[a]For explanation of feature numbers, see Table I.

In all cases, the total error in the DCS has been calculated as the resultant of all the contributing errors [i.e., $\bar{X} = (\sum_i X_i^2)^{1/2}$] and are given as the bottom row of Tables II to V.

The integral and momentum transfer cross sections were obtained by integrating the normalized DCS for each observed transition. This procedure involved a smooth extrapolation of the data to the experimentally inaccessible angles (0° and 180°) which introduced an additional small uncertainty in the integral cross sections. Although the extrapolation and resulting integration in these regions was done analytically, some uncertainty necessarily arises due to the unknown behavior of the DCS at small and large scattering angles. A conservative upper bound to the uncertainty in both the integral and momentum transfer cross sections would be an additional 5% above the value quoted for the respective DCS [e.g., 18% error for Q_i and Q_M for the $1s_2({}^1P_1)$ transition at 25-eV impact energy].

III. RESULTS AND DISCUSSION

Representative electron energy-loss spectra in neon, for two different incident electron energies and two different

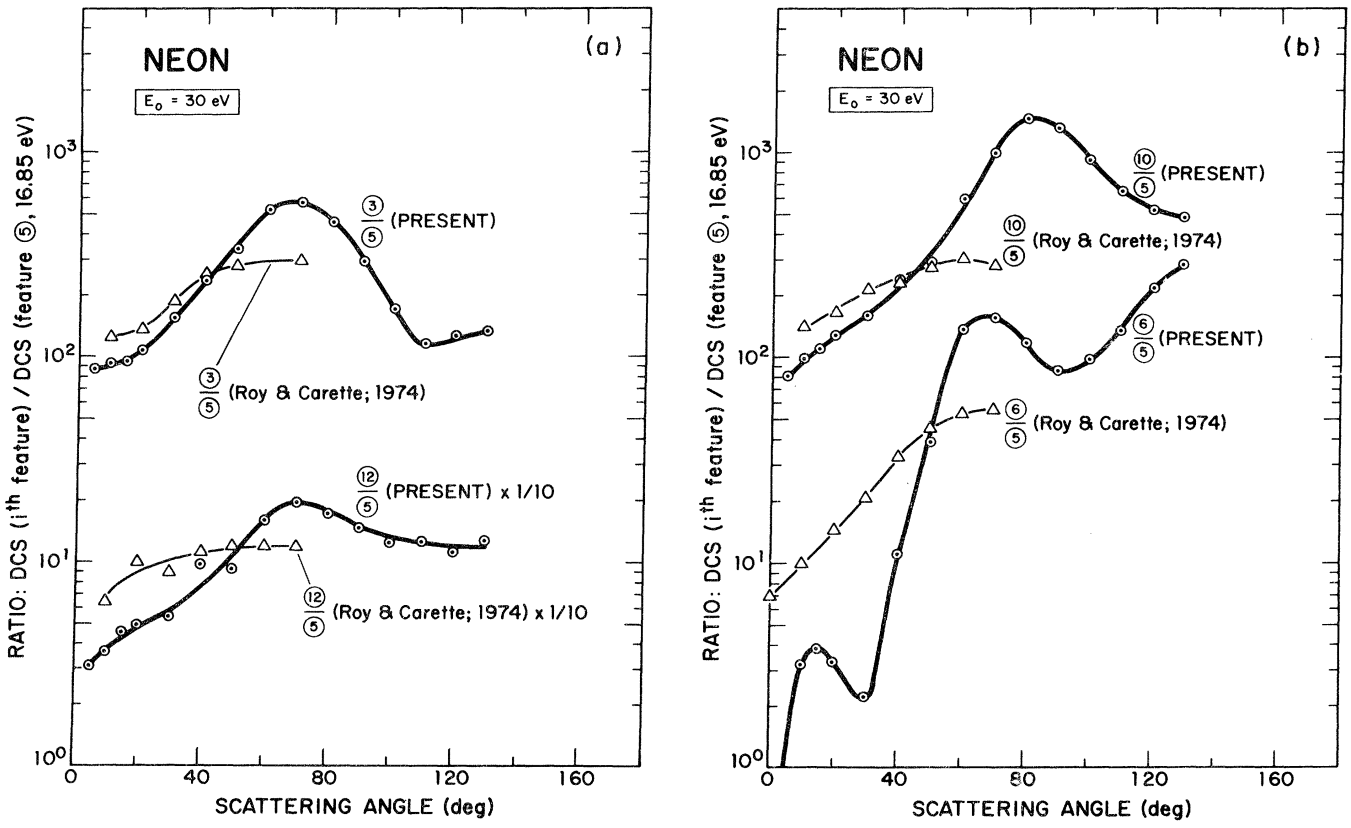

FIG. 4. (a) Ratio of the DCS for features 3 and 12 to that for feature 5 [$1s_2({}^1P_1)$], as a function of scattering angle, for an incident electron energy of 30 eV. The circles and the heavy line denote the present results and the triangles denote the results of Roy and Carette (Ref. 9). Note that all the data for feature 12 have been *reduced* by a factor of 10 before plotting for purposes of clarity. (b) Same as (a) except for features 6 and 10.

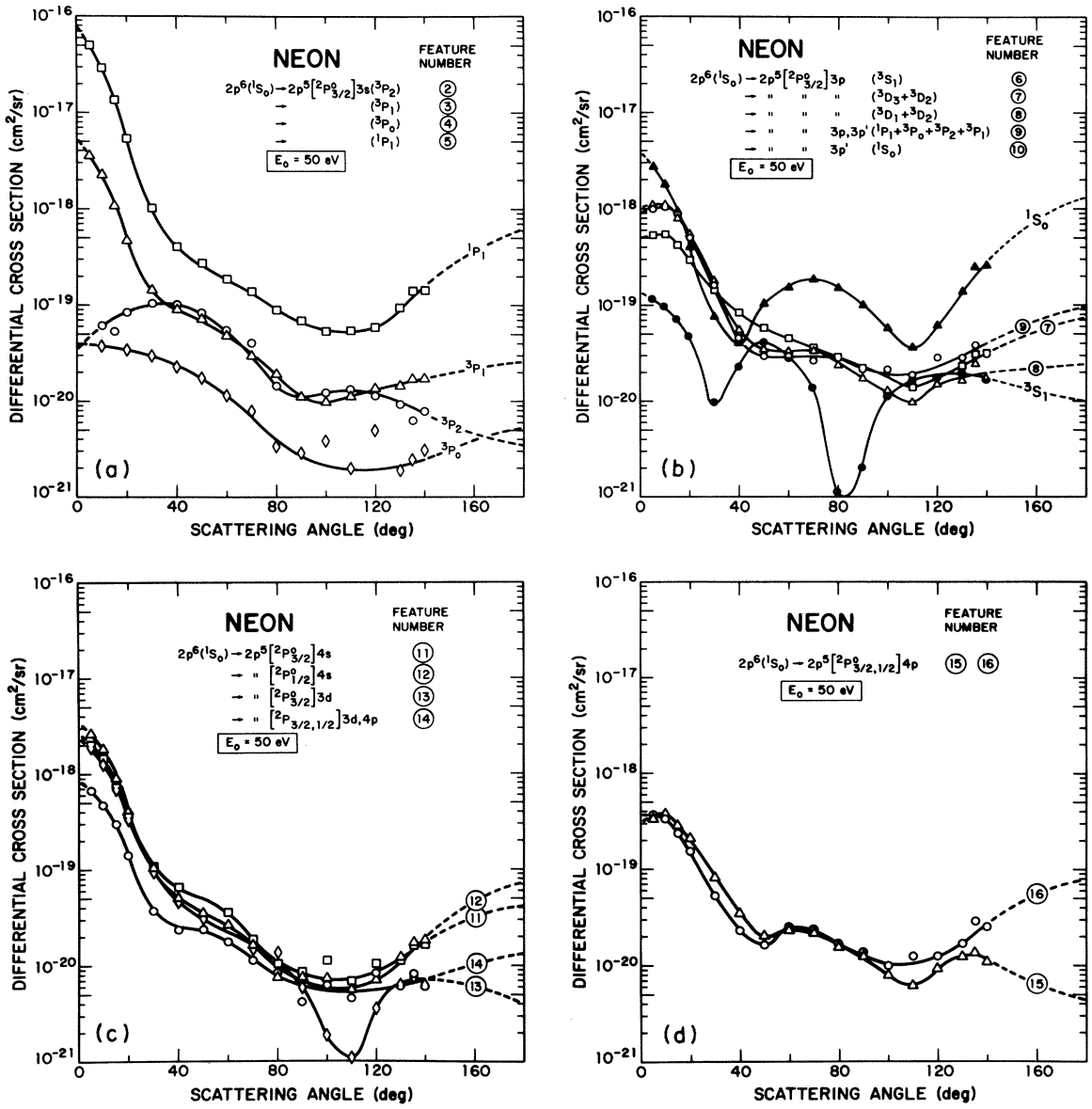

FIG. 5. (a) Absolute DCS's, as a function of scattering angle, for features 2, 3, 4, and 5, for an incident electron energy of 50 eV; (b) same as (a) except for features 6—10; (c) same as (a) except for features 11—14; (d) same as (a) except for features 15 and 16. See Table I for definition of the notation used.

scattering angles, are shown in Fig. 3 and are compared to the corresponding synthetic spectrum. For a given incident electron energy, the contribution of each electronic level to the magnitude of a particular inelastic feature, *relative* to feature 5 [the $1s_2(^1P_1)$ state], was determined at each of the scattering angles used. These data represent the fundamental information that were obtained from the electron energy-loss spectra about the excitation of individual electronic levels in neon. Some of the results obtained in this work are compared in Fig. 4 with analogous results reported by Roy and Carette.[9] In addition to covering a greater angular range, the spectral resolution employed in the present measurements was superior to that employed by Roy and Carette[9] and probably accounts for the greater variation with scattering angle of all the inelastic ratios in the present study compared to those determined by Roy and Carette.

A. Differential cross sections

Differential cross sections, for each of the 15 inelastic features (i.e., those in column 6 of Table I) were obtained by the following procedure. From the computer unfolding technique, the relative contribution of all 15 inelastic features to each electron energy-loss spectrum (i.e., fixed incident electron energy and scattering angle) was deter-

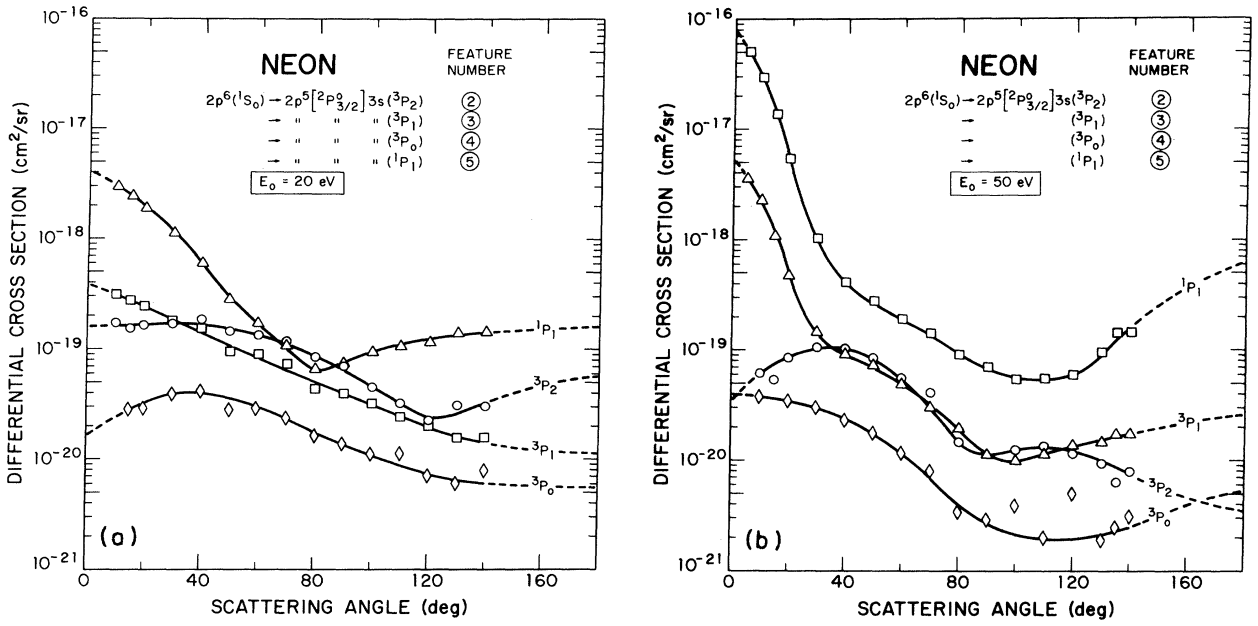

FIG. 6. (a) DCS's for excitation of features 2—5, as a function of scattering angle, for an incident electron energy of 20 eV; (b) same as (a) except for an incident electron energy of 50 eV. See Table I for definition of the notation used.

mined. These relative intensities were made absolute by calibrating the strong inelastic feature 5, that due to excitation of the $1s_2(^1P_1)$ level, against the known DCS for elastic scattering. By this normalization procedure, the relative intensities for the 15 inelastic features were converted into absolute intensities for each scattering angle

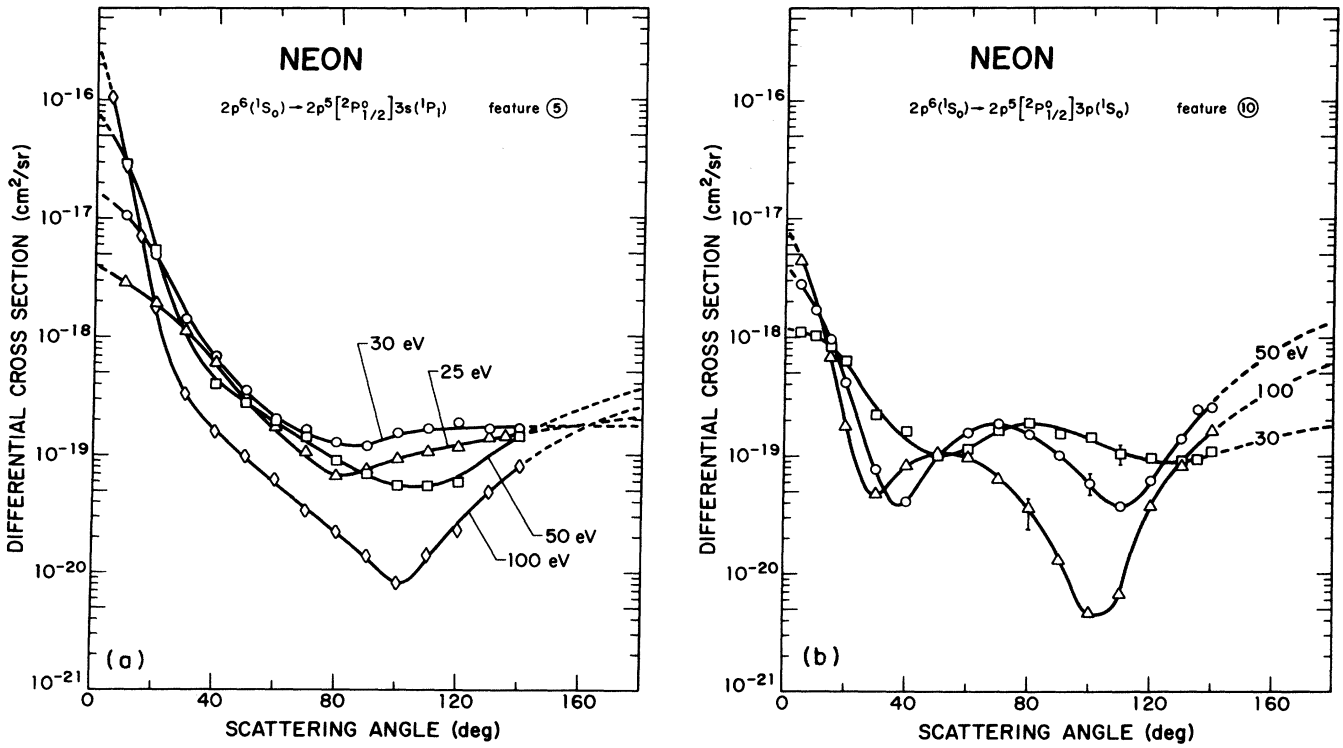

FIG. 7. (a) DCS's for excitation of feature 5, as a function of scattering angle, for incident electron energies of 25, 30, 50, and 100 eV; (b) same as (a) except for feature 10. See Table I for definition of the notation used.

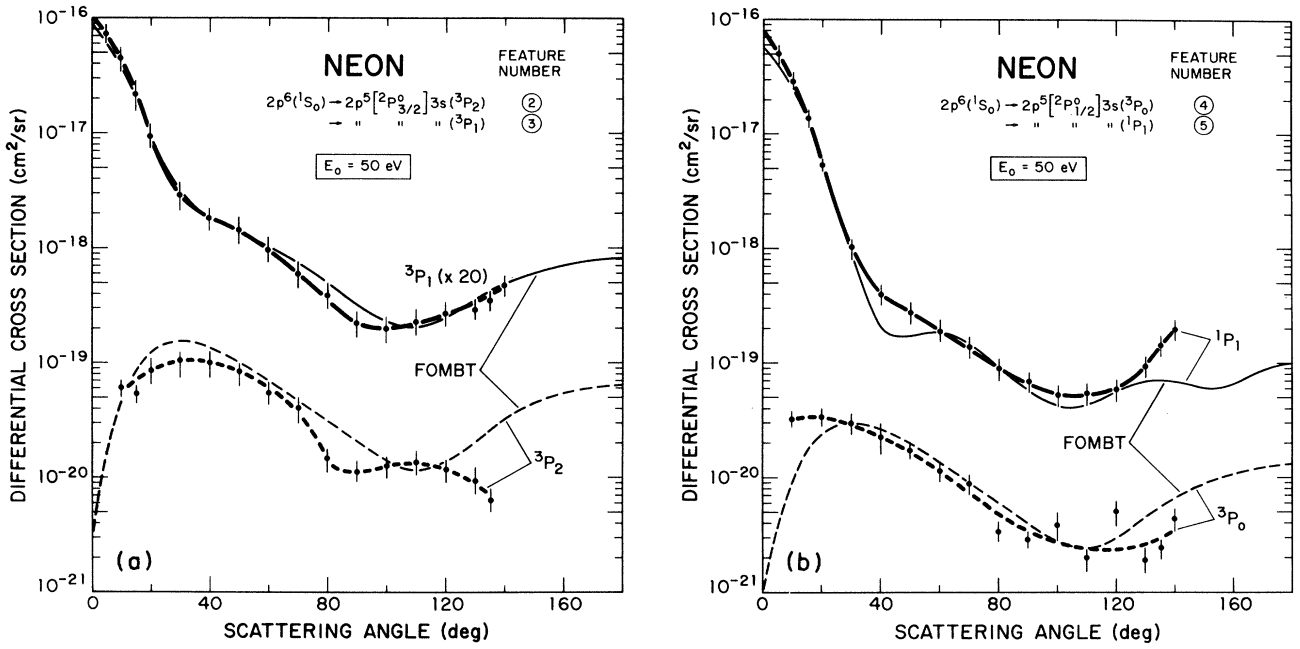

FIG. 8. (a) DCS's for electron-impact excitation of the $1s_4(^3P_1)$ and $1s_5(^3P_2)$ levels of neon, as a function of scattering angle, for an incident electron energy of 50 eV. The data points with the heavy lines denote the present experimental results while the lighter solid and dashed lines denote the results from the FOMBT (see text for details). Note that all the results for excitation of the $^3P_1$ level have been *increased* by a factor of 20 for clarity in plotting. (b) Same as (a) except for excitation of the $1s_3(^3P_0)$ and $1s_2(^1P_1)$ levels of neon.

and particular incident electron energy. This same procedure was repeated on electron energy-loss spectra taken at a number of different scattering angles to generate absolute DCS's for each inelastic feature, at a fixed incident electron energy. The resulting absolute DCS's obtained for all 15 inelastic features are illustrated in Fig. 5 for an incident electron energy of 50 eV, using the electron configuration and *LS* coupling notation as appropriate (Table I). In order to better determine if the final bound state orbital has any effect on the shape of the DCS, the results have been grouped according to excitation to the levels associated with the *K* 3s [Fig. 5(a)], 3*p* and 3*p'* [Fig. 5(b)], 4*s* and 3*d* [Fig. 5(c)], and 4*p* [Fig. 5(d)] configurations. Note that features 2, 3, 4, 5, 6, and 10 correspond to excitation of individual electronic states while the other ten features are composed of excitation of one or more electronic states (see Table I) that could not be experimentally resolved.

As might be expected, the many-electron symmetry of the final state appears to have a much greater effect on the shape of the DCS than does the symmetry of the final excited electron orbital. Three interesting characteristics of the results shown in Fig. 5 should be noted. Firstly, those resolved transitions that correspond to *dipole-forbidden* transitions from the ground state of neon (e.g., features 2 and 4) are the only ones among the 15 studied here that do not have a strong forward peak in their DCS. Features 7 and 8 (excitation of ^3D final levels), whose DCS's are more forward peaked than features 2 and 4, also show a "flattening" in their DCS's at small scattering angles. Secondly, resolved features 6 and 10, corresponding to transitions to $2p_{10}(^3S_1)$ and $2p_1(^1S_0)$, respectively, are the only transitions that contain *two* well-defined minima. This result suggests that the *S*-state many-electron symmetry of the final state might be responsible for this behavior. However, since composite features 15 and 16 show evidence for two minima, it is also possible that it is the $2p \rightarrow np'$ $(n \geq 3)$ character of these four groups of transitions that is responsible for this characteristic. Thirdly, by comparing the DCS's for features 3 $[1s_4(^3P_1)]$ and 5 $[1s_2(^1P_1)]$, one concludes that even though spin-orbit coupling in neon is quite small, it is sufficient to transform a spin-forbidden DCS (i.e., no forward peak) into one that behaves like a dipole-allowed $(J=1)$ transition.

Figure 6 illustrates the energy dependence of the DCS's for features 2–5, which correspond to the $2p^6 \rightarrow 2p^5 3s$ transitions and shows that, as the incident electron energy increases from 20 to 50 eV, the DCS's for excitation of the "dipole allowed" states $(J=1)$ becomes more forward peaked, while those for the optically forbidden transitions change relatively little. Figure 7 illustrates the energy dependence, over a larger range (25–100 eV), for features 5 $[1s_2(^1P_1)]$ and 10 $[2p_1(^1S_0)]$. The character of the DCS's do not change substantially over this energy range except that the dual minima become deeper, with increasing incident electron energy, for the $2p \rightarrow 3p$ $[2p_1(^1S_0)]$ transition (feature 10).

As mentioned in the Introduction, very little theoretical work has been reported on the DCS's for electron-impact

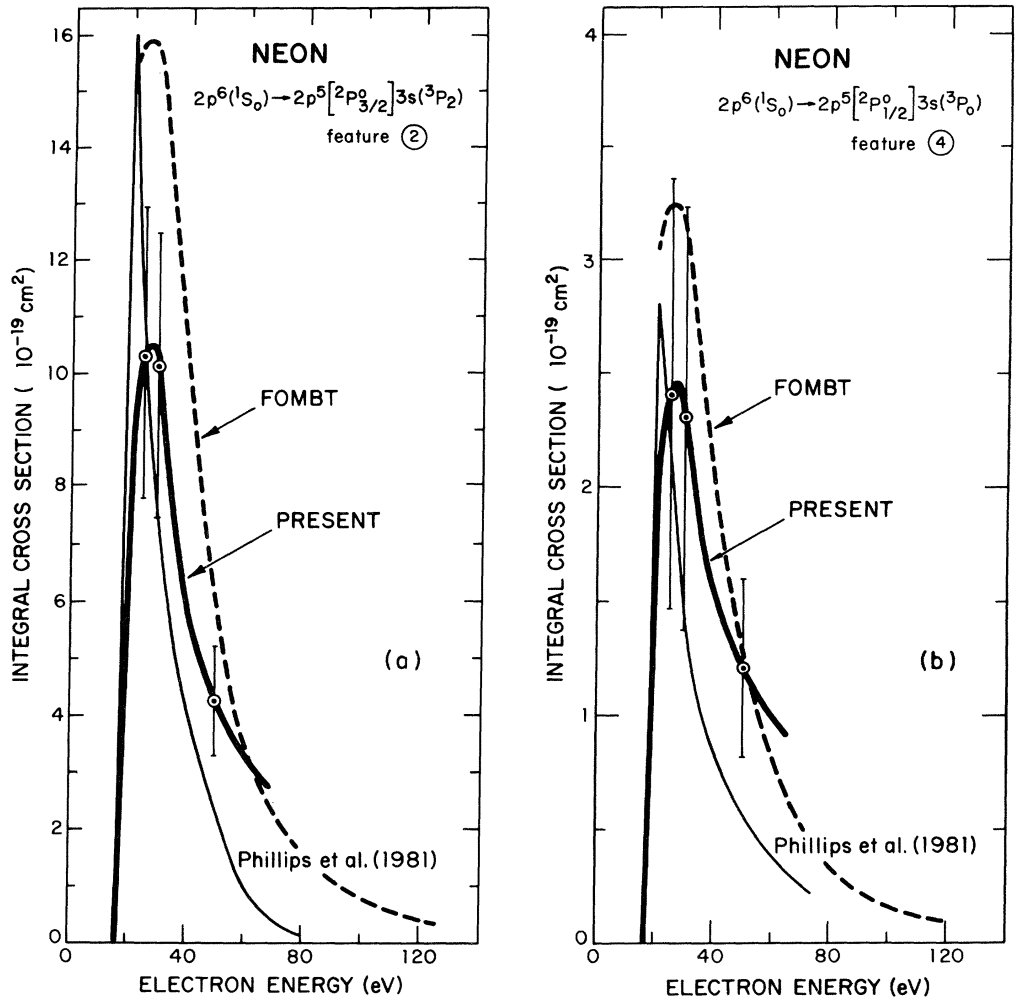

FIG. 9. (a) Integral cross section, as a function of incident electron energy for excitation of the $1s_5(^3P_2)$ level of neon. The present results are denoted by the symbols and heavy line and the lighter line shows the results of Phillips *et al.* (Ref. 20). The dashed curves denote the results (Ref. 13) from the FOMBT. (b) Same as (a) except for the $1s_3(^3P_0)$ level of neon and the lighter line denotes the results of Phillips *et al.* (Ref. 20).

excitation of neon. This situation is probably a combination of the facts that (i) no data on the absolute DCS's for excitation of the electronic levels of neon were previously available to motivate theoretical work (although some estimates of integral cross sections have been reported), and (ii) the various "first-order perturbation" approximations (Born, Glauber, impact parameter, etc.) are known to predict qualitatively and quantitatively incorrect DCS's. Due to occasional fortuitous cancellation of errors, however, the first-order perturbation models will sometimes give integral cross sections to within a factor of 2. The first-order many-body theory (FOMBT), and the related distorted-wave theory (DWT), have been very successful in predicting both the quantitative and the qualitative character of the DCS's for excitation of inelastic levels of helium[19] and argon[3(b)] in the medium energy region. This capability is illustrated in Fig. 8 in which the experimental DCS's for excitation of the lowest four excited electronic levels in neon (features 2, 3, 4, and 5) are compared to the results of the FOMBT[13] for an incident electron energy of 50 eV. As shown in the figure, the FOMBT (which has *not* been renormalized to experiment) does extremely well predicting the magnitude of both the $1s_4(^3P_1)$ and $1s_2(^1P_1)$ levels. In the case of excitation to the metastable $1s_5(^3P_2)$ and $1s_3(^3P_0)$ levels, the FOMBT again does very well in predicting both the shape and magnitude of the DCS's.

Tables II, III, IV, and V contain tabulated DCS's for excitation of the levels of neon at incident electron energies of 25, 30, 50, and 100 eV, respectively. The results summarized in these tables represent all the data obtained in this present study and show, for example, that DCS's for all 15 features were obtained only for incident electron energies of 30 and 50 eV. At 25 eV only features 2—5 were strong enough to be detected, while at 100 eV only features 5 and 10 could be measured. Note that the last

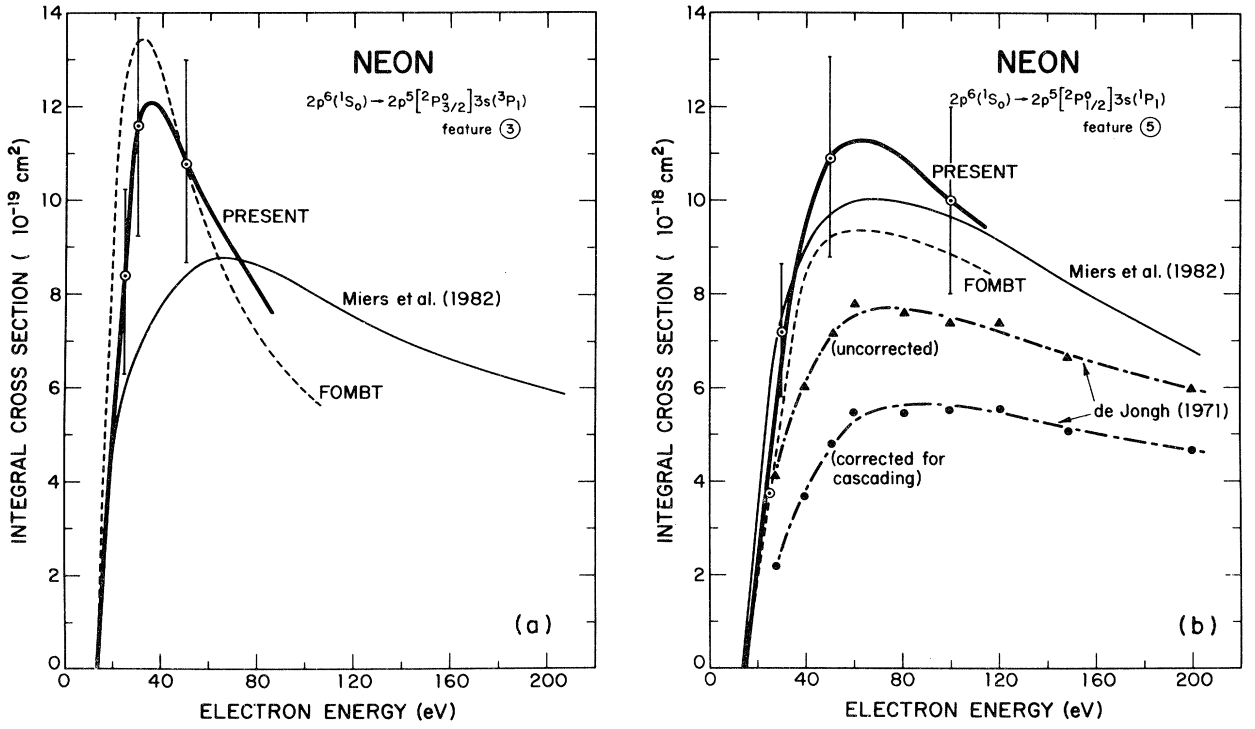

FIG. 10. (a) Integral cross section, as a function of incident electron energy, for excitation of the $1s_4(^3P_1)$ level (feature 3) of neon. The symbols and heavy line denote the present results, the lighter solid line the results of Miers *et al.* (Ref. 22), and the results (Ref. 13) of the FOMBT by the dashed line. (b) Same as (a) except for excitation of the $1s_2(^1P_1)$ level (feature 5).

entry in each column in each table contains the average error in that DCS.

B. Integral cross sections

The integral cross sections for excitation of the ith inelastic feature is obtained directly from its DCS by quadrature according to the definition

$$\sigma^i(E)=2\pi \int_{0^\circ}^{180^\circ} \frac{d\sigma^i(E,\theta)}{d\Omega} \sin\theta \, d\theta \, . \tag{1}$$

In all the results reported here, the integral cross sections were obtained by extrapolating the DCS's tabulated in Tables II—V to 0° and 180°, and then using Eq. (1). In

TABLE VI. Electron-impact inelastic integral and momentum-transfer cross sections (10^{-19} cm^2) for neon.

	Q E_0 (eV)				Q^M E_0 (eV)			
Feature[a] number	25	30	50	100	25	30	50	100
2 ($^3P_2$)	10.3	10.1	4.25		8.10	6.87	2.68	
3 ($^3P_1$)	8.40	11.6	10.8		6.40	7.29	4.13	
4 ($^3P_0$)	2.40	2.31	1.21		2.00	1.64	0.74	
5 ($^1P_1$)	37.7	72.0	109.0	100.2	26.4	40.0	33.5	16.5
6 ($^3S_1$)		3.19	2.04			3.71	1.50	
7		9.22	6.94			7.82	4.60	
8		8.73	7.62			6.63	3.14	
9		10.1	7.84			7.79	3.98	
10 ($^1S_0$)		21.3	24.3	15.1		18.6	24.5	13.1
11		6.61	7.27			4.96	3.16	
12		5.15	8.11			3.88	3.50	
13		4.54	5.70			3.36	2.13	
14		2.80	2.82			2.46	1.24	
15		5.00	3.60			4.48	1.91	
16		4.07	3.49			3.36	2.38	

[a]For explanation of feature numbers, see Table I.

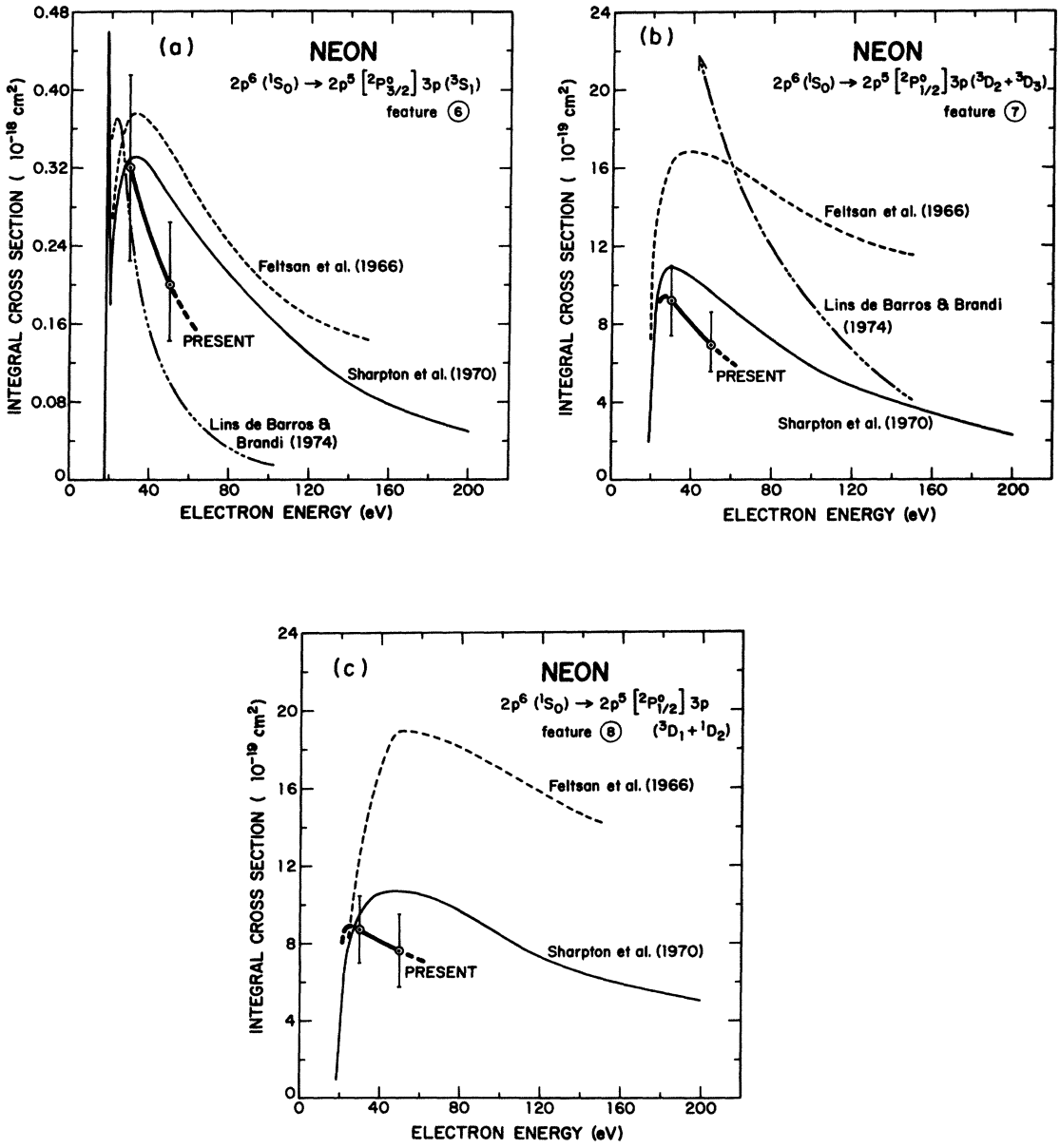

FIG. 11. (a) Integral cross section, as a function of incident electron energy, for excitation of feature 6 [$2p_{10}(^3S_1)$]. The symbols and heavy line denote the present results, and the other curves as noted in the figure (see text for details). (b) Same as (a) except for excitation of feature 7. (c) Same as (a) except for excitation of feature 8.

most cases, this extrapolation procedure introduces an error less than 5%. In this study then, integral cross sections are derived quantities rather than measured directly.

Figure 9(a) compares the integral cross section, as a function of incident electron energy, obtained in this present study for excitation of the $1s_5(^3P_2)$ with results from Phillips *et al.*[20] who used the photoemission following laser excitation from the $1s_5(^3P_2)$ state to a higher electronic state to determine the cross section. Figure 9(b) similarly compare the present results for excitation of the $1s_3(^3P_0)$ with the corresponding results from Phillips *et al.*[21] There are no other experimental data to which these present results can be compared and the agreement between the two sets of results is reasonably good, particularly since the data were obtained by such different techniques. These cross sections have the sharply peaked rapid-falloff energy dependence characteristic of strongly forbidden transitions.

Figure 10(a) compares the present integral cross-section results for excitation of the $1s_4(^3P_1)$ state with the results obtained from apparent-excitation laser-fluorescence measurements of Miers *et al.*[22] and the theoretical results from FOMBT.[13] For excitation of the $1s_2(^1P_1)$ state, comparison is also made with the apparent excitation

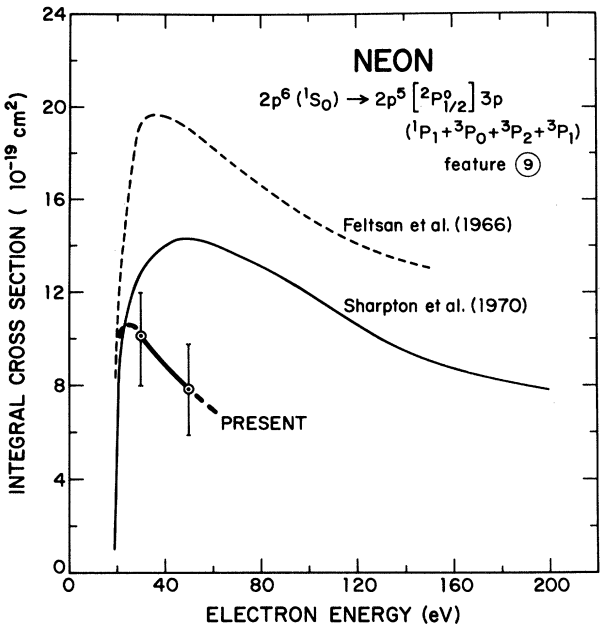

FIG. 12. Integral cross section, as a function of the incident electron energy, for excitation of feature 9 (see Table I). The symbols and heavy line denote the present results and the other curves are as noted in the figure.

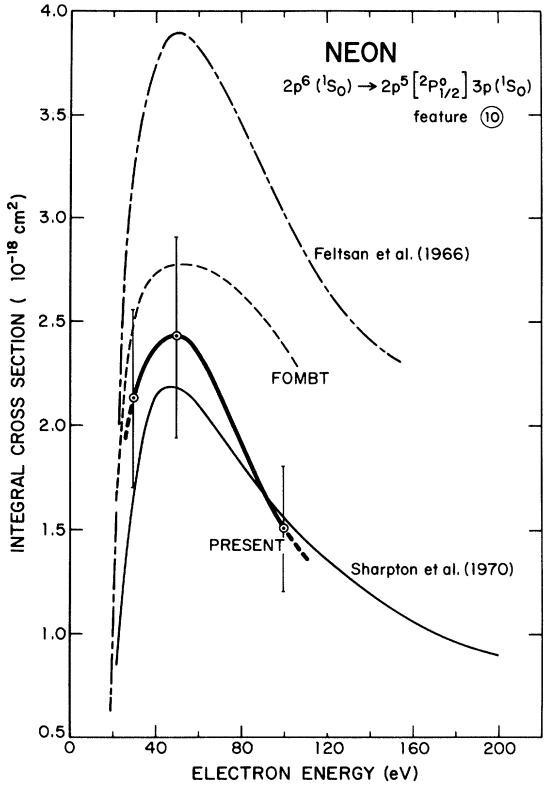

FIG. 13. Integral cross section, as a function of the incident electron energy, for excitation of feature 10 [$2p_1(^1S_0)$]. The symbols and heavy line denote the results of the present work while the other curves, obtained from apparent excitation measurements, are noted.

cross-section results of de Jongh[23] [Fig. 10(b)]. In the case of the $1s_4(^3P_1)$ excitation [Fig. 10(a)], the results of Miers *et al.*[22] are in poorer agreement with the present results than for the other states they considered and the reason for this is not known. For the $1s_2(^1P_1)$ excitation [Fig. 10(b)], the present results are in good agreement with the data from Miers *et al.*[22] but somewhat larger than the older data of de Jongh[23] who also corrected his apparent cross section for cascade from higher electronic states. For both the $1s_4(^3P_1)$ and $1s_2(^1P_1)$ excitations, the FOMBT does quite well in predicting reliable integral cross sections. It should be noted here that the integral cross sections obtained in the present study for the $1s_4(^3P_1)$ and $1s_2(^1P_1)$ excitations are generally somewhat more accurate than the others because they were well resolved in all the electron energy-loss spectra. It is quite possible that the differences between the present results for excitation of these lowest four levels in neon and the results obtained by the laser fluorescence technique are due to the uncertainties in accurately accounting for the cascading from higher electronic levels at all incident electron energies.

Figure 11 contains a comparison of the integral cross sections obtained in the present study for excitation of feature 6 [$2p_{10}(^3S_1)$], feature 7 [$2p_9(^3D_3)+2p_8(^3D_2)$], and feature 8 [$2p_7(^3D_1)+2p_6(^1D_2)$] with the corresponding results obtained from analyses of "apparent excitation" measurements by Feltsan *et al.*[24] and by Sharpton *et al.*[25] Also shown in Figs. 11(a) and 11(b) are the results obtained using a parametrization of the Born and Born-Ochkur models by Lins de Barros and Brandi.[26] As is the usual case, the results from apparent excitation measurements are larger than those obtained from electron energy-loss data because they contain some cascade contributions from higher electronic levels. Sharpton *et al.*[25] performed a very thorough analysis of their data to account for the cascade contributions and their results are only slightly larger than the present results and substantially smaller than those of Feltsan *et al.*[24] who did not correct their data for cascade contributions.

Figures 12 and 13 compare the present results for excitation of features 9 and 10, respectively, with the corresponding apparent excitation results of Feltsan *et al.*[24] and of Sharpton *et al.*[25] The results due to Feltsan *et al.*, which contain no cascade corrections, are substantially larger than the present results and those of Sharpton *et al.* The results of Sharpton *et al.*, which do contain a cascade correction, are in much better agreement with the results of the present study. It should be noted that feature 10 in the present study, corresponding to excitation of the $2p_1(^1S_0)$ state, is well resolved and strong in the electron energy-loss spectra (see Fig. 3) and is somewhat more accurately determined than some of the neighboring blended features.

Integral cross sections obtained in the present study for excitation of all the electronic levels in neon whose outer electronic configurations (Table I) are $2p^5 3s$, $2p^5 4s$, $2p^5 3p$,

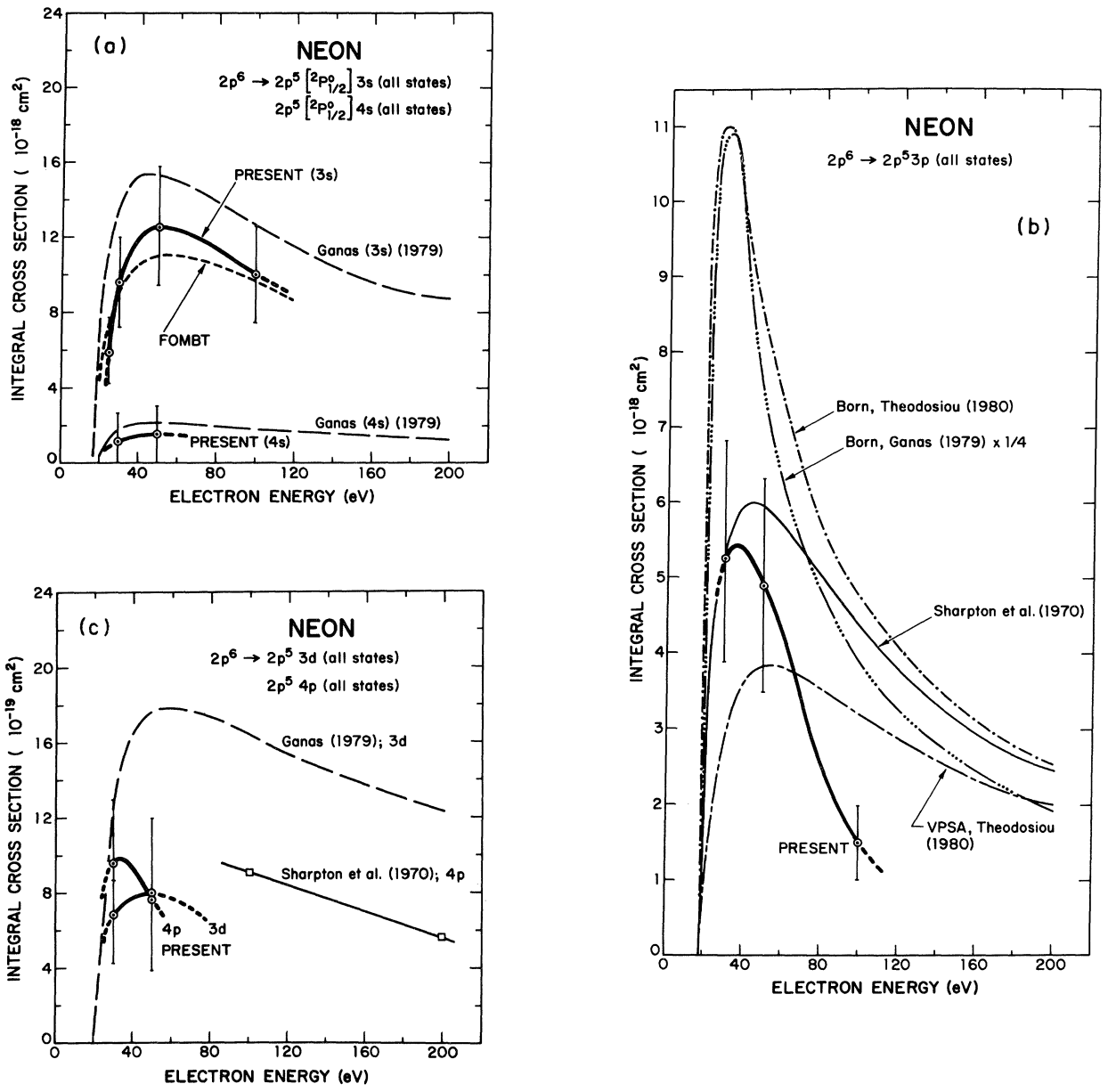

FIG. 14. (a) Integral cross section, as a function of incident electron energy, for excitation to all states with $2p^5 3s$ and $2p^5 4s$ electron configurations. The present results are denoted by the symbols and heavy line while the other curves are as noted. See Table I for the notation used. (b) Same as (a) except for levels with the electron configuration $2p^5 3p$. (c) Same as (a) except for levels with electron configurations $2p^5 3d$ and $2p^5 4p$.

$2p^5 4p$, and $2p^5 3d$ are shown in Fig. 14, where they are compared with selected theoretical and other experimental results. As in the other comparisons discussed earlier, the results of Sharpton *et al.*[25] are somewhat larger than the present results, particularly at the higher incident electron energies and probably due to cascade contributions from higher states. The theoretical results of Ganas,[27] based on an independent Born-type model are larger than the results from the present study while those from Theodosiou[28] are both larger and smaller, depending on the transition. It is unlikely that these theoretical results, which contain no details on the spin and angular momentum coupling, will give accurate cross sections.

Figure 15 is included for completeness and compares the integral cross section for excitation of all metastable levels of neon obtained by Phillips and co-workers[20–22] with that obtained by Teubner *et al.*[29] As shown in the figure, the results obtained by two different techniques are in reasonably good agreement.

Table VI contains a summary of the integral cross sections for excitation of the electronic levels in neon derived from the DCS's obtained in the present study. For completeness, Table VI also contains the "inelastic momentum transfer cross section" which can also be derived[30] from

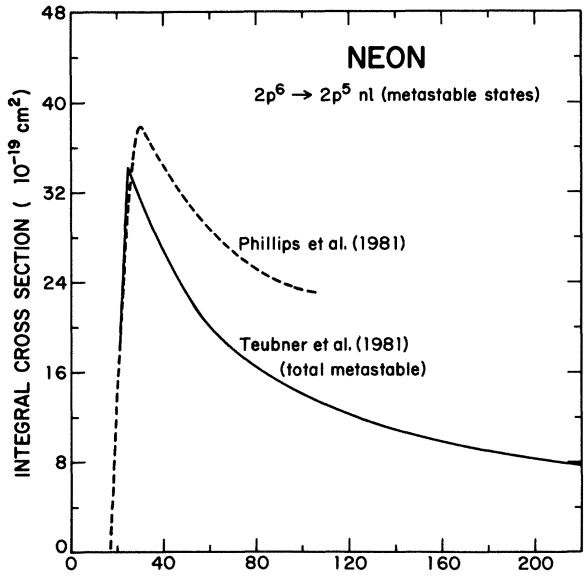

FIG. 15. Integral cross section, as a function of incident electron energy, for excitation of all metastable levels of neon. The sources of the data plotted are as noted.

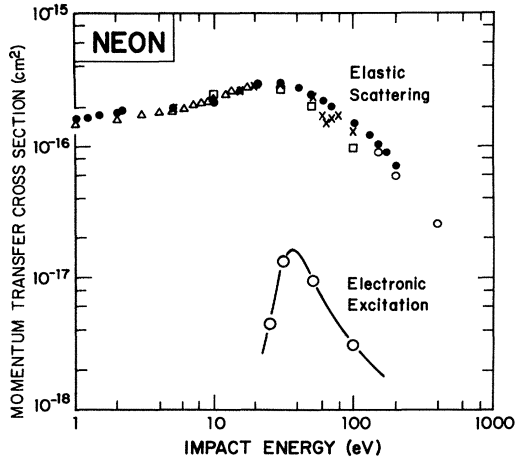

FIG. 16. Integral momentum transfer cross section for neon as a function of incident electron energy. The data points in the upper portion of the figure are various measurements of the momentum transfer due to elastic scattering and are discussed in detail in Ref. 6. The open circles and connecting line represent the momentum transfer due to inelastic scattering derived in this study.

the appropriate DCS and Fig. 16 plots these data along with the momentum transfer cross section due to elastic scattering.[6]

ACKNOWLEDGMENTS

The authors thank Dr. George Csańak for a number of suggestions that improved the clarity of this paper. One of us (D.C.C.) gratefully acknowledges the National Science Foundation International Programs Office for partial support of this research. The research described in this paper was performed at the Jet Propulsion Laboratory, California Institute of Technology under contract with the National Aeronautics and Space Administration.

[1]S. E. Moody, L. A. Levin, R. E. Center, J. J. Ewing, and E. L. Klosterman, IEEE J. Quantum Electron. QE-17, 1856 (1981); C. Brau, in *Excimer Lasers, Topics in Applied Physics,* edited by C. K. Rhodes (Springer, Berlin, 1979), Vol. 30, p. 87.

[2]B. H. Bransden and M. R. C. McDowell, Phys. Rep. 46, 249 (1978).

[3](a) A. Chutjian and D. C. Cartwright, Phys. Rev. A 23, 2178 (1981); (b) N. T. Padial, G. D. Meneses, F. J. da Paixão, G. Csańak, and D. C. Cartwright, *ibid.* 23, 2194 (1981).

[4]S. K. Srivastava, H. Tanaka, A. Chutjian, and S. Trajmar, Phys. Rev. A 23, 2156 (1981).

[5]S. Trajmar, S. K. Srivastava, H. Tanaka, H. Nishimura, and D. C. Cartwright, Phys. Rev. A 23, 2167 (1981).

[6]D. F. Register and S. Trajmar, preceding paper [Phys. Rev. A 29, 1785 (1984)].

[7]F. H. Nicoll and C. B. O. Mohr, Proc. Roy. Soc. A 142, 647 (1933).

[8]W. C. Tam and C. E. Brion, J. Elec. Spec. Rel. Phen. 2, 111 (1973).

[9]D. Roy and J. D. Carette, Can. J. Phys. 52, 1178 (1974).

[10]F. J. de Heer, R. H. J. Jansen, and W. van der Kaay, J. Phys. B 12, 979 (1979).

[11]R. W. Wagenaar and F. J. de Heer, J. Phys. B 13, 3855 (1980).

[12]W. E. Kauppila, T. S. Stein, J. H. Smart, M. S. Dababneh, Y. K. Ho, J. P. Downing, and V. Pol, Phys. Rev. A 24, 725 (1981).

[13]L. E. Machado, E. P. Leal, and G. Csańak, following paper [Phys. Rev. A 29, 1811 (1984)].

[14]S. W. Jensen, Ph.D. Thesis, University of California, Riverside, 1978 (unpublished).

[15]S. Trajmar and D. F. Register, in *Electron Molecule Collisions,* edited by K. Takayanagi and I. Shimamura, (Plenum, New York, to be published).

[16]R. T. Brinkman and S. Trajmar, J. Phys. E 14, 245 (1981).

[17]D. C. Cartwright, A. Chutjian, S. Trajmar, and W. Williams, Phys. Rev. A 16, 1013 (1977).

[18]D. F. Register, H. Nishimura, and S. Trajmar, J. Phys. B 13, 1651 (1980).

[19]L. D. Thomas, G. Csańak, H. S. Taylor, and B. S. Yarlagadda, J. Phys. B 7, 1719 (1974); G. D. Meneses, N. T. Padial, and G. Csańak, *ibid.* 11, L237 (1978).

[20]M. H. Phillips, L. W. Anderson, and C. C. Lin, Phys. Rev. A 23, 2751 (1981).

[21]M. H. Phillips, L. W. Anderson, C. C. Lin, and R. E. Miers, Phys. Lett. 82A, 404 (1981).

[22]R. E. Miers, J. E. Gastineau, M. H. Phillips, L. W. Anderson, and C. C. Lin, Phys. Rev. A 25, 1185 (1982).

[23]J. P. de Jongh, Ph.D. thesis, University of Utrecht, 1971 (un-

published).
[24]P. V. Feltsan, I. P. Zapesochny, and M. M. Pouch, Ukr. Fiz. Zh. 11, 1222 (1966).
[25]F. A. Sharpton, R. M. St. John, C. C. Lin, and F. E. Fajen, Phys. Rev. A 2, 1305 (1970).
[26]H. G. P. Lins de Barros and H. S. Brandi, Can. J. Phys. 53, 689 (1975).
[27]P. S. Ganas, Mol. Phys. 38, 1127 (1979).
[28]C. E. Theodosiou, J. Phys. B 13, L113 (1980).
[29]P. J. O. Teubner, J. L. Riley, M. C. Tonkin, J. E. Furst, and S. J. Buckman, *Abstracts of the XII International Conference on the Physics of Electronic and Atomic Collisions, Gatlinburg, Tennessee, 1981,* edited by S. Datz (North-Holland, Amsterdam, 1981), p. 153.
[30]D. C. Cartwright, J. App. Phys. 49, 3855 (1978).